Journal of Thermal Analysis and Calorimetry (2023) 148:2367–2375
https://doi.org/10.1007/s10973-022-11889-1

Thermal arrest analysis of the reverse martensitic transformation in a $Ni_{55}Fe_{19}Ga_{26}$ Heusler alloy obtained by melt-spinning

A. Vidal-Crespo[1] · A. F. Manchón-Gordón[2] · J. S. Blázquez[1] · J. J. Ipus[1] · P. Svec[3] · C. F. Conde[1]

Received: 22 August 2022 / Accepted: 10 December 2022 / Published online: 30 December 2022

Abstract

$Ni_{55}Fe_{19}Ga_{26}$ ribbons obtained by melt-spinning technique exhibit a martensitic transformation from $L2_1$ cubic austenite phase to 14 M martensite phase above room temperature. We have taken advantage of the existence of thermal hysteresis of the martensitic phase transition (~ 11 K) to analyze the effect of isothermal treatments on the reverse martensitic transformation, which has been analyzed by means of interrupted heating using differential scanning calorimetry. The experimental findings clearly indicate a time-depending effect in the martensitic transformation at temperatures between the austenite start and finish temperatures. Moreover, it has been observed that two successive martensitic transformations take place after the isothermal arrest was performed.

Keywords Thermal arrest · Martensitic transformation · Calorimetry · Ni–Fe–Ga Heusler alloys · Rapid solidification techniques

Introduction

Martensitic transformation (MT) is a first-order phase transition which occurs in the solid state from a high temperature (high symmetry) austenite phase to a low temperature (low symmetry) martensite phase. This kind of transformation, which has attracted considerable attention since the discovery of the shape memory effect and superelastic behavior in Ti–Ni alloys in the early 1960s [1], has been traditionally classified into two groups, athermal and isothermal transformations [2]. In the case of athermal transformations, the amount of the product phase only depends on temperature but not time. This is due to a diffusionless character of MT as the composition of the product is the same as that of the original phase. In fact, this transformation is characterized by a collective motion of a relatively large number of atoms with a velocity approaching that of sound waves [2]. However, debates about the time-dependence of these transformations arise because some experimental results indicate the occurrence of isothermal character in the MTs in different Heusler [3–6] and TiNi-based alloys [7–9]. Although commercial TiNi-based alloys are the most preferred in different applications due to their unique properties of shape memory effect and superelasticity, these alloys have high costs and hard fabrication process disadvantages [10, 11]. As an alternative to these compounds, Cu-based shape memory alloys have been widely studied due to their low cost and relatively simple processing [10, 12–14]. Besides the traditional, thermally induced, shape memory effect found in TiNi-based alloys, in 1996, Ullako [15] presented a faster and precise control of the shape memory effect in ferromagnetic materials, leading to the magnetic shape memory effect branch. The most representative family system corresponds to Ni–Mn–Ga alloys [16].

A large number of applications are based on the solid-state martensitic transformation of this kind of materials. Therefore, it is of importance to understand the martensitic transformation and its stability against thermal treatments around the transition temperature range in the alloy of interest. The present work aims to provide experimental insight on the subtle effects of isothermal treatments during MT occurring in a Ni–Fe–Ga Heusler alloy, which has

✉ A. F. Manchón-Gordón
alejandro.manchon@icmse.csic.es

1 Dpto. Física de la Materia Condensada, ICMSE-CSIC, Universidad de Sevilla, P.O. Box 1065, 41080 Seville, Spain

2 Instituto de Ciencia de Materiales de Sevilla, ICMSE CSIC-Universidad de Sevilla, C. Américo Vespucio 49, 41092 Seville, Spain

3 Institute of Physics, Slovak Academy of Sciences, Dúbravská Cesta 9, 845 11 Bratislava 45, Slovak Republic

been proposed as an alternative to Ni–Mn–Ga for magnetic refrigeration due to its improved ductility [16]. In this sense, the presence of gamma phase precipitates (beneficial for mechanical properties but detrimental for magnetic ones) is found in conventionally produced samples, but rapidly quenched melt-spun ribbons present a monophasic character from X-ray studies [17–19]. Therefore, controlled thermal treatments would lead to optimize the amount of gamma phase and, as a consequence, melt-spun Heusler alloys are widely produced to study these systems. However, the metastable character of the obtained samples leads to both reversible and irreversible changes during the thermal treatments even at temperatures in the range of MT, which deserves a deeper analysis to which the present work is devoted.

Previous studies on the thermally induced MT in Ni–Fe-Ga system have shown that the austenite exhibits $L2_1$ structure and transforms to martensite monoclinic modulated 14 M structure [19]. However, the martensitic phase can undergo an inter-martensitic transformation (IMT) under applied stress from 14 M phase to the non-modulated $L1_0$ structure [19, 20]. Although several observations have been made for Ni–Fe–Ga melt-spun ribbons [17–19, 21–23], the effect of isothermal treatments on the martensitic transformation of these compounds seems to be neglected in the literature. In this study, we have undertaken an extensive analysis of the MT in a $Ni_{55}Fe_{19}Ga_{26}$ Heusler alloy prepared by melt-spinning. To do that, we have explored the thermal arrest of the development of $L2_1$ structure during reverse MT and its effect on this transformation.

Experimental

The material used in the present study is a $Ni_{55}Fe_{19}Ga_{26}$ (at. %) ribbon prepared by melt-spinning technique. The preparation procedure and a detailed microstructural characterization (including Mössbauer spectroscopy) and stability of melt-spun ribbon (which are the same that have been employed in this study) can be found in [19]. Magnetic characterization of the ribbons can be found in [21].

MT of the ribbons was characterized by means of differential scanning calorimetry analysis using a Perkin-Elmer DSC7 (Perkin-Elmer, Norwalk, CT, USA) under Ar flow equipped with a cooling system. Different heating rates (β from 5 to 80 K min^{-1}) and different times (from 0 to 120 min) were used for non-isothermal and isothermal treatments, respectively. Measured temperature was corrected at different heating rates using the melting temperature of In (429.75 K) standard (errors below 0.5 K). DSC calibrations at the different heating rates were performed.

The samples were firstly subjected to a heating of 473 K in order to eliminate the dependence of the MT on the strain fields present in the ribbons. In fact, it has been shown that for melt-spun ribbons, MT shifts to lower temperatures as the samples have been previously heated up to higher temperatures (in the range 473 K to 623 K, below the temperature of the formation of the gamma phase) [19]. However, when the maximum temperature reached is the same, the transformation keeps constant. This phenomenon has been associated to the lattice relaxation by the attenuation of the quenched-in strains stored in ribbons during the processing. In fact, it is known that the production of Heusler alloys by rapid quenching techniques leads to a strong dispersion of the parameters characterizing the martensitic transformation [23]. This dispersion is attenuated after heat treatments leading to a relaxation of the stored stresses [23, 24]. Therefore, to avoid the dispersion in the characteristic parameters of the martensitic transformation due to inhomogeneities and the transformational changes caused by cycling [23], the same pieces of ribbon has been used in all DSC measurements. The mass of the analyzed pieces of the ribbons was around the same of the In standard employed to the calibration of the equipment (~ 20 mg). Due to the small mass of one piece with the dimension of the crucible of the equipment, several pieces of the ribbon (5–6) were introduced for each experiment in order to obtain a similar mass of the employed standards.

The isothermal behavior of the MT was analyzed through DSC experiments. The experiments were conducted at a heating/cooling rate of 20 K min^{-1}. The heating rate was chosen in order to optimize the signal–noise ratio of the DSC measurements. Typical values of heating rates in the calorimeter used are between 5 and 80 K min^{-1}. As heating rate increases, heat flux signal increases accordingly but temperature gradients should also increase. For these measurements, the isothermal process, between austenite start and austenite finish temperatures, was interrupted at different stages of the transformation temperature range followed by cooling to room temperature (RT). Afterward, subsequent heating process up to 473 K and cooled down to RT was performed. In order to clarify the followed process, Fig. 1 shows, as an example, the temperature–time curve of a complete DSC experiment including the isothermal experiment performed at 388 K interrupted after 30 min.

Results and discussion

The characteristic transition temperatures consisting of the austenite start, A_s, and finish temperatures, A_f, upon heating are determined by DSC (β = 10 K min^{-1}) to be 380 and 400 K, respectively, while the forward transformation upon cooling are 385 and 355 K, respectively [23]. MT temperatures can vary in a certain range of temperature which depends on the temperature heating rate [23, 25, 26]. Therefore, calorimetric measurements with heating rates from 5 to

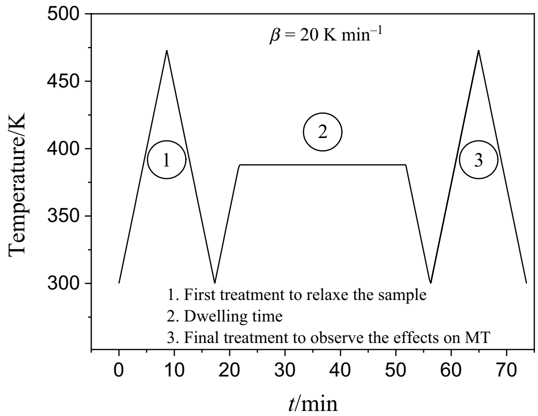

Fig. 1 Example of a complete thermal treatments carried out in DSC experiments. Firstly, a heating treatment is performed to relax the sample (1). On the second heating, the experiment was stopped at 388 K for 30 min (2). Subsequently, the sample was cooled to RT and heated again up to 473 K (3). The experiments were conducted at a heating/cooling rate of 20 K min^{-1}

80 K min^{-1} were made in order to identify the dependence of the MT temperature interval [13]. Figure 2 shows the fitted linear relationship between the values of A_s and A_f as well as the peak temperature, A_{peak}, of the transformation and heating rate. Both A_s and A_f were estimated as the intersection between the corresponding maximum slopes with the baseline. A shift to higher temperatures as β increases can be observed for both A_{peak} and A_f, indicating the thermally activated character of the MT. However, it can be observed that β has a minor influence on A_s. Therefore, the transformation temperature interval (ΔT=A_f-A_s) increases with β and shifts to higher temperatures. From the intersection of the fittings ($\beta \to 0$ K min^{-1}), A_f and A_s reaches 398.0 ± 0.5 and 386.4 ± 0.5 K, respectively, and ΔT=11.6 K (its minimum value). The obtained results are in agreement with the findings of Wang et *al.*, indicating that the heating rates results in larger variation of A_f than A_s in TiNiCu shape memory alloys [27]. Similar results can be also found in Ni–Fe–Ga Heusler alloys [28]. Due to the specific shape of the ribbons, it was necessary to introduce several pieces in each experiment, leading to a worst thermal contact between the crucible and the sample. This could be, partially, the responsible of the widening of the range of the reverse transformation observed in Fig. 2.

The apparent activation energy, E_a, in the MT of Heusler alloys, is generally obtained by Kissinger method [25, 29]. However, when the dependence of activation energy on the heating rate is analyzed, it is possible to predict a temperature at which the MT would be athermal ($E_a \approx 0$). In the case of the studied sample, this temperature has been previously calculated, reaching 428 ± 8 K [23]. Therefore, an isothermal character of the MT would be expected at temperatures below 428 K.

Figure 3 shows the corresponding plots for Kissinger [30, 31] and Augis-Bennett [32] models to estimate the effective activation energy. Despite the resulting values are roughly in agreement (500 ± 80 and 350 ± 70 kJ mol^{-1} for Kissinger and Augis-Bennet methods, respectively), it is worth mentioning that both agree describing the deviation from linearity as heating rate increases. This trend can be interpreted as a complex character of the transition, which could include athermal (null activation energy) and isothermal

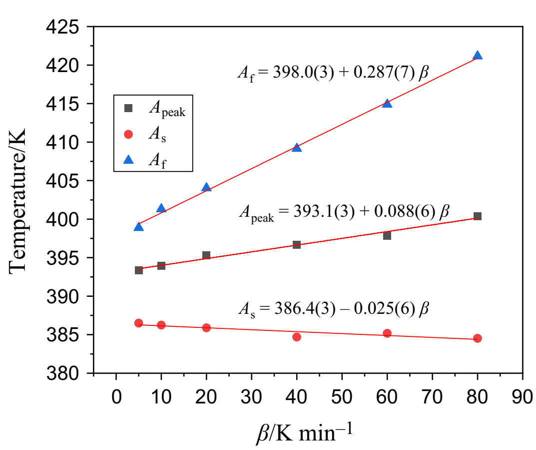

Fig. 2 Linear relationship between heating rates and characteristic temperatures of the martensitic transformation. DSC curves of $Ni_{55}Fe_{19}Ga_{26}$ recorded at different heating rates around MT can be found in [13]

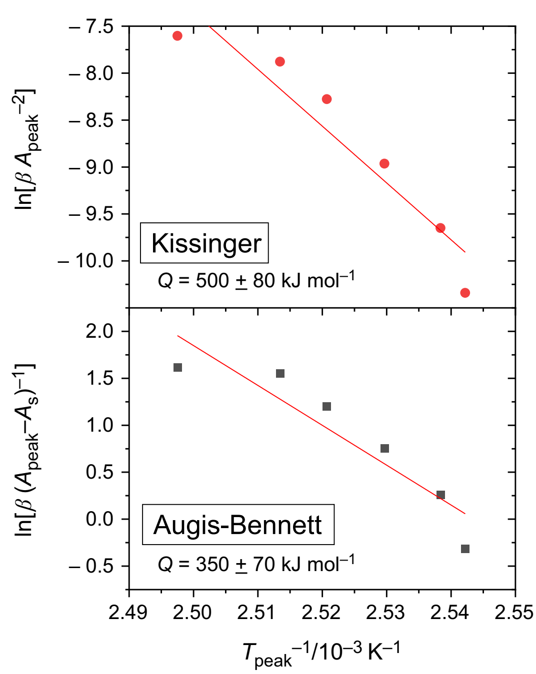

Fig. 3 Kissinger and Augis-Bennett plots for the peak temperature of the martensitic transformation

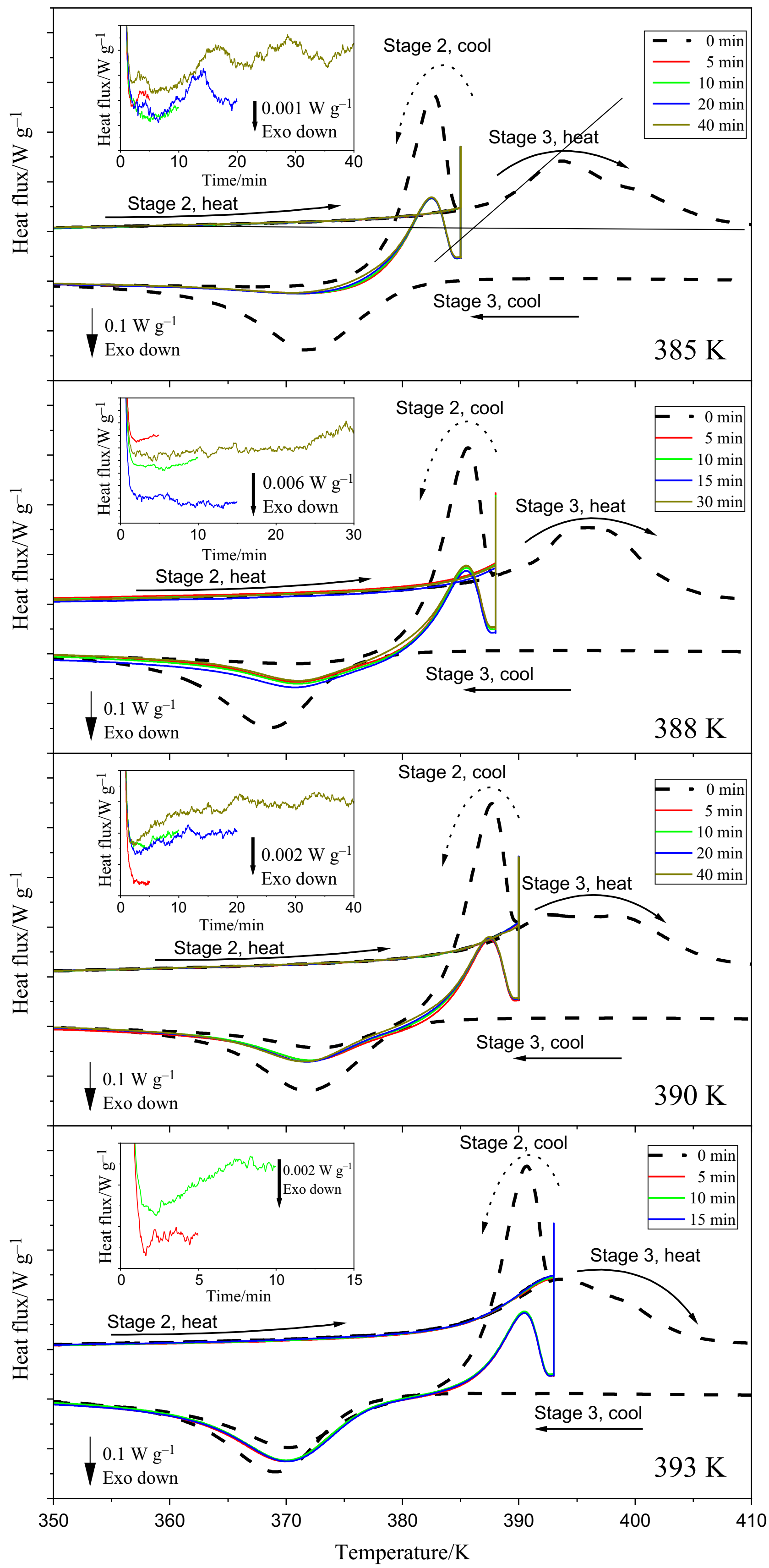

Fig. 4 Interrupted differential scanning calorimetry measurements of the transformation behavior at 20 K min^{-1} at the indicated temperatures and times. Full subsequent heating/cooling curves from stage 3 are shown only for 0 min annealing for convenience. First stage corresponds to the first treatment performed to relax the sample (see Fig. 1)

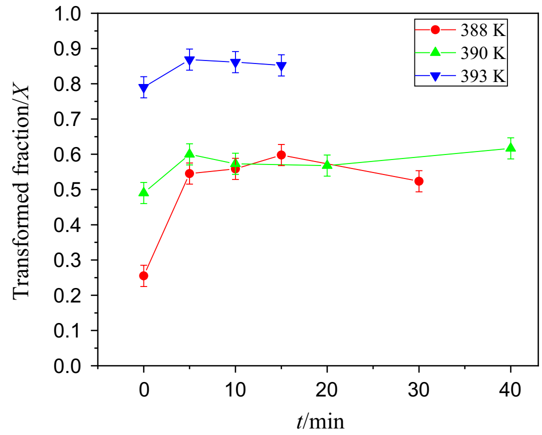

Fig. 5 Transformed fraction obtained as the relative enthalpy to the total of complete process as a function of isothermal time

phenomena. As heating rate increases, higher temperatures are reached, and isothermal contributions are speeded up, whereas athermal contributions are completed at their respective temperatures. This different behavior may explain why Kissinger and Augis-Bennett plots do not lead to a good linearity and indicates that the effective activation energy must be taken with care in this process.

In order to determine the nature of the MT, in situ DSC interrupted experiments were conducted at temperatures between A_s and A_f. Relaxed sample was heated up to the selected temperature (385, 388, 390 and 393 K) with a rate of 20 K min^{-1} and then holding at this temperature for different dwelling times. DSC results of Fig. 4 show that a certain volume fraction of austenite phase has been formed during the dwelling time (evidenced from the enhancement of the exothermic peaks upon cooling). Insets of Fig. 4 show the corresponding isothermal DSC signal. The weakness of the signal prevents further analysis of them.

The transformed fraction, X, developed during dwelling could be approximated to relative enthalpy to the total one of the processes as $X = \Delta H(T)/\Delta H_{total}$, where $\Delta H(T)$ is the enthalpy developed up to temperature T after the dwelling time and ΔH_{total} in the total enthalpy of the martensitic process without thermal arrest. After all the isothermal experiments were performed, the sample was heated up to 973 K to decrease the martensitic transformation temperature below room temperature. All the features found in the original curves vanish in the subsequent cycle, which was used as the corresponding baseline. The dependence of the transformed fraction with the dwelling time at different temperatures is shown in Fig. 5. The baseline could not be determined for the case of the isothermal treatments at 385 K, as the martensitic transformation process is incomplete in the studied temperature range. For that reason, results corresponding to this temperature has not been included. Although the obtained values can be only considered as a rough estimation of the transformed fraction, a clear time effect is observed; an increase in the transformed fraction with the increase in dwelling time is achieved. Similar results have been previously reported for the martensitic transformation of Ni–Mn–In Heusler alloys at lower heating/cooling rates (β=10 K min^{-1}) [26]. In this sense, the effect of the heating rate on the increase in the transformed fraction can be neglected. In any case, it is not possible to achieve the complete martensitic transformation with the performed thermal treatments.

The occurrence of the apparent time effect does not necessarily confirm the isothermal nature of the MT. In fact, there exist different factors that may contribute to the observed time-dependence of a particular transformation. Most of them include relaxation processes that occur during dwelling due to the interaction between the crystal lattice defects and moving phase interfaces [8, 9, 33] and the development of strain nanodomains [34]. In fact, isothermal MT was observed in non-stoichiometric Ti–Ni alloys but not found in the equiatomic TiNi alloy [34]. This phenomenon was associated to the formation of strain nanodomains and the existence of substitutional atoms. In the Ni-rich Ni–Fe–Ga ribbons studied here, the accumulation of the elastic energy due to a large concentration of substitutional atoms and the typical disorder of these compounds prepared by melt-spinning [35] could be the reason for a partial development of the reverse MT at constant temperature. In this sense, it has been shown that the substitution of Fe by Mn in $Ni_{55}Fe_{19}Ga_{26}$ alloy leads to change in its microstructure and phase structure behaviors [36].

The effect of interrupting the heating during the reverse MT on the complete transformation have been investigated on DSC completing the MT after the interrupted scans. Figure 6 shows DSC measurements of the MT of the studied alloy after the interrupted scans at different temperatures and times. Again, remarkable effects on the MT can be observed. In this case, DSC curves show two overlapped endothermic peaks on heating, whose deconvolution can be obtained with the increase in the dwelling time for isothermal treatments performed at temperatures lower than 393 K. Moreover, it can be observed that the fraction ascribed to each transformation depends on the temperature at which the isothermal treatment was performed. From the viewpoint of the thermodynamics, the martensitic transformation required an overheating to A_S or an undercooling to M_S from the equilibrium temperature, T_o, in order to initiate the transformation between austenite and martensite. T_o can be evaluated approximately as $(M_S+A_f)/2$ [37], resulting 392.5 K for the studied alloy at $\beta = 20$ K min^{-1}. In this sense, it has been proven that isothermal reverse martensitic transformations are possible between M_S and T_o [38]. Our results would suggest that isothermal reverse martensitic transformations are

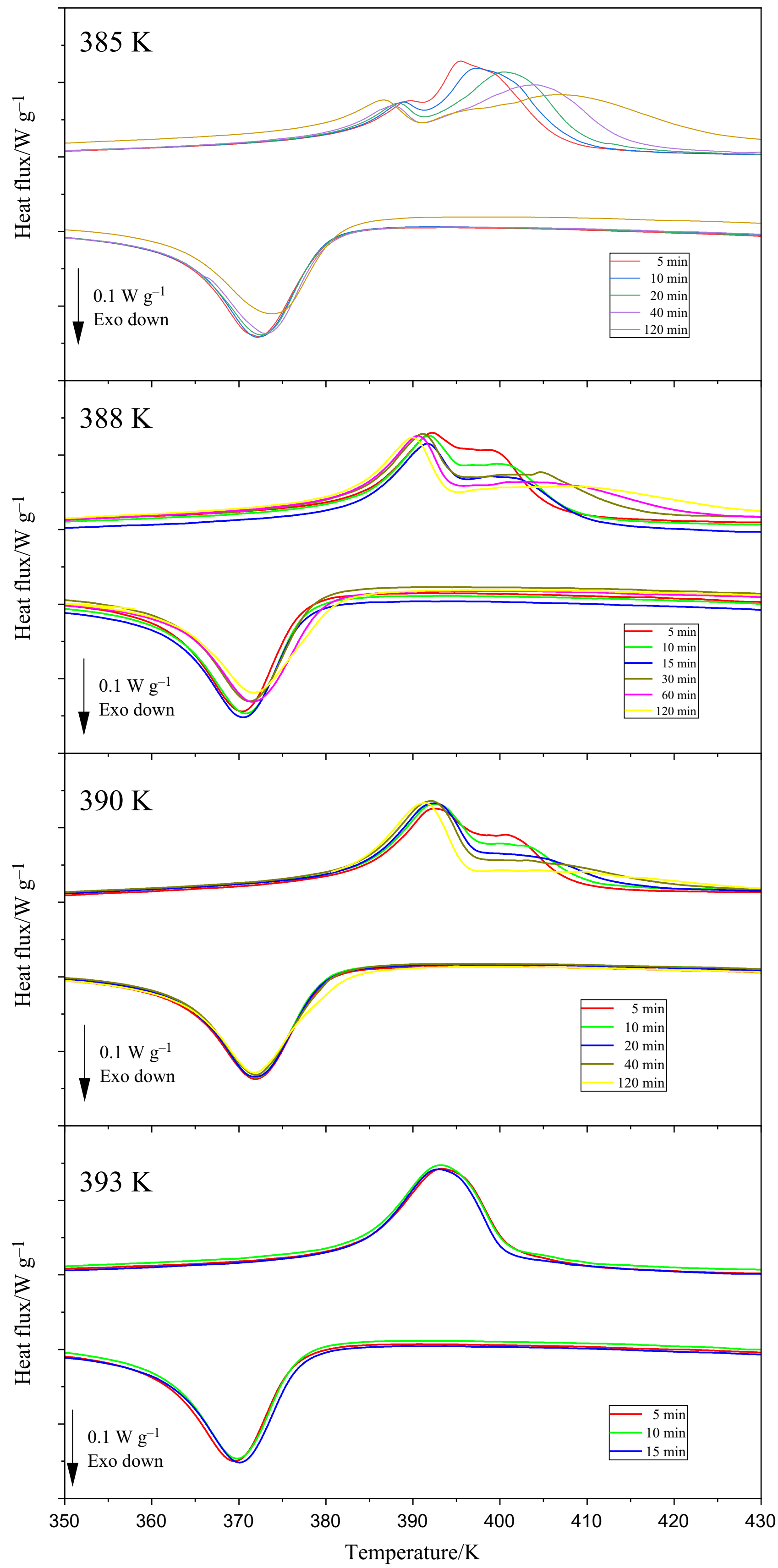

Fig. 6 Transformation behavior of the $Ni_{55}Fe_{19}Ga_{29}$ alloy measured after interrupted heating at the indicated temperatures and times

only possible between A_S and T_o. On the one hand, the effect of increase the dwelling time at this temperature is minimum (see Fig. 4). On the other hand, the deconvolution observed in the other cases, is not observed when the isothermal treatments are performed at this temperature.

The obtained results are similar to those reported in works that study the effect of interruption of martensitic transformation, which confirmed that partial transformation cycles can affect transformation behavior in shape memory alloys significantly in the subsequent complete transformation cycle [39–41]. This phenomenon has been called temperature memory effect (TME) [39], thermal arrest memory effect [40] or step-wise martensite to austenite reversible transformation [41]. In these studies, it has been shown that if the reverse transformation of a shape memory alloy is arrested at a temperature between A_S and A_f, a kinetic stop, closely related to the previous arrested temperature, appears in the next complete transformation, in agreement with the obtained results. Although the TME was firstly observed in Ti–Ni alloys [41], it has been also reported in Ni–Mn–Ga Heusler alloys [42]. This phenomenon has been explained as follows: if the MT is interrupted at a certain temperature, the martensite phase partly transforms to austenite phase but some martensite phase could remain, which we would called M_1. Cooling the sample down to temperatures below M_f, new martensite phase is formed, M_2, which could have different preferential orientation structure. Therefore, there would exist domains of both martensite phase variants. If the alloy, containing the two variants, is heated again, it would transform to austenite phase. However, both variants would transform at different temperatures due to M_1 overcomes more work produced by the domain walls [42]. This effect is observed in Fig. 6, in which the DSC scans in the austenite formation range clearly depends on the dwelling time. In fact, the deconvolution of the MT leads to the broadening of the phase transformation temperature span. The increase in the domain walls between the different martensite variants with the increase in the dwelling time could be the responsible of the observed broadening.

The occurrence of the multi-stage transformation of the reverse MT could be also attributed to the development of inter-martensitic transitions. However, in situ X-ray diffraction (XRD) experiments as a function of temperature did not show evidences for such IMT in these alloys, in the case of as-spun ribbons [13]. Nevertheless, martensitic phases can undergo inter-martensitic transitions under applied compressive or tensile stress [19, 20]. In this sense, IMT between the modulated and the non-modulated martensite phases, caused by changes in composition, temperature and external stress, has been extensively investigated in Ni–Mn–Ga alloys [43–47]. Although in these alloys the IMT generally takes place at much lower temperatures than the MT, the IMT can be tuned to be close to the MT, and hence forming two successive magneto-structural transformations, as it has been found in $Ni_{55.5}Mn_{17.8}Ga_{26.7}$ alloy [48]. In these systems, the coexistence of two successive magneto-structural transformations enhances the magnetocaloric properties compared with those observed in other Ni-Mn based alloys under similar conditions and without IMT [49, 50]. The phenomenon observed in our DSC measurements in the Ni–Fe–Ga alloy is different from the results described in previous investigations, where the IMT occurs both cooling and heating processes [47, 48]. However, the occurrence of the two successive transformations only in heating regimen has been previously reported in $Ni_{45}Ti_{51.8}Fe_{3.2}$ shape memory alloy, which was attributed to the creation of local stress fields due to the formation of precipitates [51]. In the present case, a higher deconvolution of the MT is obtained with the increase in the dwelling time, but only at temperatures below 390 K. It is worth mentioning that the analysis of the dependence of the activation energy on temperature and the heating rate predicts a temperature at which the MT would be athermal, 428 ± 8 K [23]. In any case, independently of the degree of deconvolution of the MT process, the total enthalpy developed during the complete reverse martensitic transformation is 6.5 ± 1.0 J g^{-1}.

Conclusions

Isothermal arrests have been conducted within the temperature window of the reverse martensitic transformation in a melt-spun $Ni_{55}Fe_{19}Ga_{26}$ Heusler alloy. Differential scanning calorimetry results allow detecting a time effect on the martensitic transformation and provides a way to decouple two successive magneto-structural processes in the reverse transformation. Therefore, the isothermal experiments are not only an interesting way to determine the nature of the martensitic transformation but also broadening the phase transformation temperature span of the martensite to austenite phase transformation. These experimental findings can help to develop more efficiently caloric materials with such a kind of Heusler alloy system.

In this work we could not overcome the problems concerning in situ X-ray diffraction analysis. The time required for data acquisition, in the order of the dwelling times performed here for isothermal treatments, prevent us from a comparative analysis between XRD and DSC data. Further studies on much faster microstructural techniques (e.g., synchrotron based ones) could clarify the experimental findings reported in this study. In this study we have limited to thermal treatment effects. However, the magnetically/mechanically induced character of the MT would make interesting future studies on the effect of other external factors (pressure or magnetic field application).

Acknowledgments This work was supported by AEI/FEDER-UE (Projects US-1260179 and P18-RT-746) and the PAI of the Regional Government of Andalucía. A. Vidal-Crespo acknowledges a VPPI-US fellowship. P. Svec acknowledges support of the projects APVV-19-0369 and VEGA 2/0144/21.

Authors' contributions AV-C contributed to experiments, formal analysis, writing—original draft; AFM-G contributed to conceptualization, experiments, formal analysis, writing—original draft; JSB contributed to conceptualization, methodology, supervision, resources, writing—review and editing; JJI contributed to supervision, writing—review and editing; PS contributed to samples, resources, supervision, writing—review and editing; CFC contributed to resources, methodology, supervision, writing—review and editing.

Funding Funding for open access publishing: Universidad de Sevilla/CBUA.

References

1. Buehler WJ, Gilfrich JV, Wiley RC. Effect of low-temperature phase changes on the mechanical properties of alloys near composition TiNi. J Appl Phys. 1963;34:1475–7. https://doi.org/10.1063/1.1729603.
2. Christian JW. The theory of transformations in metals and alloys: equilibrium and general kinetic theory. 2nd ed. Oxford: Pergamon Press; 1975.
3. Hürrich C, Roth S, Pötschke M, Rellinghaus B, Schultz L. Isothermal martensitic transformation in polycrystalline $Ni_{5.0}Mn_{2.9}Ga_{2.1}$. J Alloys Compd. 2010;494:40–3. https://doi.org/10.1016/j.jallcom.2010.01.044.
4. Ito W, Umetsu RY, Kainuma R, Kakeshita T, Ishida K. Heat-induced and isothermal martensitic transformations from kinetically arrested parent phase in NiCoMnIn metamagnetic shape memory alloy. Scr Mater. 2010;63:73–6. https://doi.org/10.1016/j.scriptamat.2010.03.010.
5. Lee Y, Todai M, Okuyama T, Fukuda T, Kakeshita T, Kainuma R. Isothermal nature of martensitic transformation in an $Ni_{45}Co_5Mn_{36.5}In_{13.5}$ magnetic shape memory alloy. Scr Mater. 2011;64:927–30. https://doi.org/10.1016/j.scriptamat.2010.12.030.
6. Lino-Zapata FM, Yan HL, Ríos-Jara D, Sánchez Llamazares JL, Zhang YD, Zhao X, Zuo L. Characterization of the kinetic arrest of martensitic transformation in $Ni_{45}Co_5Mn_{36.8}In_{13.2}$ melt-spun ribbons. J Magn Magn Mater. 2018;446:253–9. https://doi.org/10.1016/j.jmmm.2017.09.037.
7. Xue S, Wang W, Wu D, Zhai Q, Zheng H. On the explanation for the time-dependence of B2 to R martensitic transformation in $Ti_{50}Ni_{47}Fe_3$ shape memory alloy. Mater Lett. 2012;72:119–21. https://doi.org/10.1016/j.matlet.2011.12.095.
8. Salas D, Cesari E, Van Humbeeck J, Kustov S. Isothermal B2–B19′ martensitic transformation in Ti-Rich Ni–Ti shape memory alloy. Scr Mater. 2014;74:64–7. https://doi.org/10.1016/j.scriptamat.2013.10.022.
9. Kustov S, Salas D, Santamarta R, Cesari E, Van Humbeeck J. Isothermal and athermal martensitic transformations in the B2–R–B19′ sequence in Ni–Ti shape memory alloys. Scr Mater. 2010;63:1240–3. https://doi.org/10.1016/j.scriptamat.2010.08.047.
10. Silva DDS, Guedes NG, Oliveira DF, Torquarto RA, Júnior FWELA, Lima BASG, Feitosa FRP, Gomes RM. Effects of long-term thermal cycling on martensitic transformation temperatures and thermodynamic parameters of polycrystalline CuAlBeCr shape memory alloy. J Therm Anal Calorim. 2022;2022(147):7875–81. https://doi.org/10.1007/s10973-021-11106-5.
11. Mohd Khalil AN, Azmi AI, Murad MN, Mahboob Ali MA. The effect of cutting parameters on cutting force and tool wear in machining nickel titanium shape memory alloy ASTM F2063 under minimum quantity nanolubricant. Procedia CIRP. 2018;77:227–30. https://doi.org/10.1016/j.procir.2018.09.002.
12. Aksu Canbay C, Aydoğdu A. Thermal analysis of Cu-14.82 wt% Al-0.4 wt% be shape memory alloy. J Therm Anal Calorim. 2013;113:731–7. https://doi.org/10.1007/s10973-012-2792-6.
13. Andrade BHS, Silva DDS, Brito ICA, Caluête RE, Sousa ARR, Gomes RM, Oliveira DF. Influence of strain rate on mechanical properties of a CuAlMnTiB shape memory alloy. J Mater Res Technol. 2022;16:1667–72. https://doi.org/10.1016/j.jmrt.2021.12.100.
14. Pedrosa MTMA, Silva DDS, Brito ICA, Alves RF, Caluête RE, Gomes RM, Oliveira DF. Effects of hot rolling on the microstructure, thermal and mechanical properties of CuAlBeNbNi Shape Memory alloy. Thermochim Acta. 2022;711:179188. https://doi.org/10.1016/j.tca.2022.179188.
15. Ullakko K. Magnetically controlled shape memory alloys: a new class of actuator materials. J Mater Eng Perform. 1996;5:405–9. https://doi.org/10.1007/BF02649344.
16. Pons J, Cesari E, Seguí C, Masdeu F, Santamarta R. Ferromagnetic shape memory alloys: alternatives to Ni–Mn–Ga. Mater Sci Eng A. 2008;481–482:57–65. https://doi.org/10.1016/j.msea.2007.02.152.
17. Álvarez-Alonso P, Aguilar-Ortiz CO, Villa E, Nespoli A, Flores-Zúñiga H, Chernenko VA. Conventional and Inverse elastocaloric effect in Ni–Fe–Ga and Ni–Mn–Sn ribbons. Scr Mater. 2017;128:36–40. https://doi.org/10.1016/j.scriptamat.2016.09.033.
18. Villa E, Aguilar-Ortiz CO, Nespoli A, Álvarez-Alonso P, Camarillo-Garcia JP, Salazar D, Passaretti F, Flores-Zúñiga H, Hosoda H, Chernenko VA. Tailoring thermomechanical treatment of Ni–Fe–Ga melt-spun ribbons for elastocaloric applications. J Mater Res Technol. 2019;8:4540–6. https://doi.org/10.1016/j.jmrt.2019.07.067.
19. Manchón-Gordón AF, Ipus JJ, Kowalczyk M, Wójcik A, Blázquez JS, Conde CF, Maziarz W, Švec P Sr, Kulik T, Conde A. Effect of pressure on the phase stability and magnetostructural transitions in nickel-rich NiFeGa ribbons. J Alloys Compd. 2020;844:156092. https://doi.org/10.1016/j.jallcom.2020.156092.
20. Hamilton RF, Sehitoglu H, Efstathiou C, Maier HJ. Inter-Martensitic transitions in Ni–Fe–Ga single crystals. Acta Mater. 2007;55:4867–76. https://doi.org/10.1016/j.actamat.2007.05.003.
21. Manchón-Gordón AF, Ipus JJ, Kowalczyk M, Blázquez JS, Conde CF, Švec P, Kulik T, Conde A. Comparative study of structural and magnetic properties of ribbon and bulk Ni55Fe19Ga26 Heusler alloy. J Alloys Compd. 2021;889:161819. https://doi.org/10.1016/j.jallcom.2021.161819.

22. Okumura H, Uemura K. Influence of quenching rate on the magnetic and martensitic properties of Ni–Fe–Ga melt-spun ribbons. J Appl Phys. 2010;108:43910. https://doi.org/10.1063/1.3465613.
23. Manchón-Gordón AF, López-Martín R, Ipus JJ, Blázquez JS, Svec P, Conde CF, Conde A. Kinetic analysis of the transformation from 14M Martensite to L21 Austenite in Ni–Fe–Ga melt spun ribbons. Met. 2021;11:849.
24. Tolea F, Sofronie M, Crisan AD, Enculescu M, Kuncser V, Valeanu M. Effect of thermal treatments on the structural and magnetic transitions in melt-spun Ni–Fe–Ga–(Co) ribbons. J Alloys Compd. 2015;650:664–70. https://doi.org/10.1016/j.jallcom.2015.07.296.
25. Zheng H, Wu D, Xue S, Frenzel J, Eggeler G, Zhai Q. Martensitic transformation in rapidly solidified Heusler $Ni_{49}Mn_{39}Sn_{12}$ ribbons. Acta Mater. 2011;59:5692–9. https://doi.org/10.1016/j.actamat.2011.05.044.
26. Zheng H, Wang W, Wu D, Xue S, Zhai Q, Frenzel J, Luo Z. Athermal nature of the Martensitic transformation in Heusler alloy Ni–Mn–Sn. Intermetallics. 2013;36:90–5. https://doi.org/10.1016/j.intermet.2013.01.012.
27. Wang ZG, Zu XT, Huo Y. Effect of heating/cooling rate on the transformation temperatures in TiNiCu shape memory alloys. Thermochim Acta. 2005;436:153–5. https://doi.org/10.1016/j.tca.2005.06.028.
28. Yu HJ, Zu XT, Fu H, Zhang XY, Wang ZG. Effect of annealing and heating/cooling rate on the transformation temperatures of NiFeGa alloy. J Alloys Compd. 2009;470:237–40. https://doi.org/10.1016/j.jallcom.2008.03.063.
29. Recarte V, Pérez-Landazábal JI, Ibarra A, Nó ML, San Juan J. High temperature β phase decomposition process in a Cu–Al–Ni shape memory alloy. Mater Sci Eng A. 2004;378:238–42. https://doi.org/10.1016/j.msea.2003.09.111.
30. Kissinger HE. Variation of peak temperature with heating rate in differential thermal analysis. J Res Natl Bur Stand. 1956;57:217. https://doi.org/10.6028/jres.057.026.
31. Kissinger HE. Reaction kinetics in differential thermal analysis. Anal Chem. 1957;29:1702–6. https://doi.org/10.1021/ac60131a045.
32. Augis JA, Bennett JE. Calculation of the Avrami parameters for heterogeneous solid state reactions using a modification of the Kissinger method. J Therm Anal. 1978;13:283–92. https://doi.org/10.1007/BF01912301.
33. Kustov S, Salas D, Cesari E, Santamarta R, Van Humbeeck J. Isothermal and athermal martensitic transformations in Ni–Ti shape memory alloys. Acta Mater. 2012;60:2578–92. https://doi.org/10.1016/j.actamat.2012.01.025.
34. Resnina N, Belyaev S, Shelyakov A. Isothermal B2→B19′ Martensitic transformation in $Ti_{40.7}Hf_{95}Ni_{44.8}Cu_5$ shape memory alloy. Scr Mater. 2016;112:106–8. https://doi.org/10.1016/j.scriptamat.2015.09.024.
35. Zhang H-R, Wu G-H. Atomic-size effect on the microstructural properties of Ni_2FeGa. Acta Mater. 2011;59:1249–58. https://doi.org/10.1016/j.actamat.2010.10.057.
36. Sarkar SK, Biswas A, Babu PD, Kaushik SD, Srivastava A, Siruguri V, Krishnan M. Effect of partial substitution of Fe by Mn in $Ni_{55}Fe_{19}Ga_{26}$ on its microstructure and magnetic properties. J Alloys Compd. 2014;586:515–23. https://doi.org/10.1016/j.jallcom.2013.10.057.
37. Tang W, Sundman B, Sandström R, Qiu C. New Modelling of the B2 phase and its associated martensitic transformation in the Ti–Ni system. Acta Mater. 1999;47:3457–68. https://doi.org/10.1016/S1359-6454(99)00193-7.
38. Pérez-Reche FJ, Vives E, Mañosa L, Planes A. Athermal character of structural phase transitions. Phys Rev Lett. 2001;87:195701. https://doi.org/10.1103/PhysRevLett.87.195701.
39. Wang ZG, Zu XT, Fu YQ, Wang LM. Temperature memory effect in TiNi-based shape memory alloys. Thermochim Acta. 2005;428:199–205. https://doi.org/10.1016/j.tca.2004.11.018.
40. Madangopal K, Banerjee S, Lele S. Thermal arrest memory effect. Acta Metall Mater. 1994;42:1875–85. https://doi.org/10.1016/0956-7151(94)90012-4.
41. Airoldi G, Corsi A, Riva G. Step-wise martensite to austenite reversible transformation stimulated by temperature or stress: a comparison in NiTi alloys. Mater Sci Eng A. 1998;241:233–40. https://doi.org/10.1016/S0921-5093(97)00494-2.
42. Zhou MZ, Zhang X, Meng XL, Cai W, Zhao LC. Temperature memory effect induced by incomplete transformation in Ni–Mn–Ga-based shape memory alloy. Mater Today Proc. 2015;2:S867–70. https://doi.org/10.1016/j.matpr.2015.07.419.
43. Chernenko VA, Seguí C, Cesari E, Pons J, Kokorin V. V sequence of martensitic transformations in Ni–Mn–Ga alloys. Phys Rev B. 1998;57:2659–62. https://doi.org/10.1103/PhysRevB.57.2659.
44. Kokorin VV, Perekos AO, Tshcherba AA, Babiy OM, Efimova TV. Intermartensitic phase transitions in Ni–Mn–Ga alloy, magnetic field effect. J Magn Magn Mater. 2006;302:34–9. https://doi.org/10.1016/j.jmmm.2005.08.010.
45. Çakır A, Righi L, Albertini F, Acet M, Farle M, Aktürk S. Extended investigation of intermartensitic transitions in Ni–Mn–Ga magnetic shape memory alloys: a detailed phase diagram determination. J Appl Phys. 2013;114:183912. https://doi.org/10.1063/1.4831667.
46. Li Z, Xu K, Zhang Y, Tao C, Zheng D, Jing C. Two successive magneto-structural transformations and their relation to enhanced magnetocaloric effect for $Ni_{55.8}Mn_{18.1}Ga_{26.1}$ Heusler alloy. Sci Rep. 2015;5:15143. https://doi.org/10.1038/srep15143.
47. Hu F, Wei S, Cao Y, Li Z, He X, Xu K, Zhang Y, Kang Y, Yang H, Zhang Q. Magnetocaloric and barocaloric effects associated with two successive magnetostructural transformations in $Ni_{55.5}Mn_{17.8}Ga_{26.7}$ alloy. J Alloys Compd. 2020;818:153356. https://doi.org/10.1016/j.jallcom.2019.153356.
48. Hu F, Wei S, He X, Li Z, Xu K, Cao Y, Kang Y. Enhanced magnetocaloric effects driven by two successive magneto-structural transformations in $Ni_{55.5}Mn_{17.8}Ga_{26.7}$ Alloy under hydrostatic pressure. Solid State Commun. 2019;300:113691. https://doi.org/10.1016/j.ssc.2019.113691.
49. Fabbrici S, Kamarad J, Arnold Z, Casoli F, Paoluzi A, Bolzoni F, Cabassi R, Solzi M, Porcari G, Pernechele C, et al. From direct to inverse giant magnetocaloric effect in Co-doped NiMnGa multifunctional alloys. Acta Mater. 2011;59:412–9. https://doi.org/10.1016/j.actamat.2010.09.059.
50. Dey S, Singh S, Roy RK, Ghosh M, Mitra A, Panda AK. Influence of Mn incorporation for Ni on the magnetocaloric properties of rapidly solidified off-stoichiometric NiMnGa ribbons. J Magn Magn Mater. 2016;397:342–6. https://doi.org/10.1016/j.jmmm.2015.08.102.
51. Zhang Y, Jiang S, Zhu X, Zhao Y, Liang Y, Sun D. Influence of Fe addition on phase transformation behavior of NiTi shape memory alloy. Trans Nonferrous Met Soc China. 2017;27:1580–7. https://doi.org/10.1016/S1003-6326(17)60179-1.